Single-vortex dynamics in resistively shunted Josephson junction arrays

1997 J. Phys.: Condens. Matter 9 2571

(http://iopscience.iop.org/0953-8984/9/12/006)

J. Phys.: Condens. Matter **9** (1997) 2571–2583. Printed in the UK PII: S0953-8984(97)76610-4

Single-vortex dynamics in resistively shunted Josephson junction arrays

José C Ciria† and C Giovannella†‡

† Dipartimento di Fisica and Sezione INFN dell'Università di Roma Tor Vergata, Via della Ricerca Scientifica 1, 00133 Roma, Italy

‡ Sezione INFM dell'Università di Roma Tor Vergata, Via della Ricerca Scientifica 1, 00133 Roma, Italy

Received 23 July 1996, in final form 20 December 1996

Abstract. We have numerically solved the equation of motion for a single vortex in a resistively shunted Josephson junction array. The vortex velocity (v), the damping coefficient (η) and the dynamical barrier for the cell-to-cell vortex motion (E_b) are studied. In particular, we have focused our attention on their dependence on the bias current (i_{dc}), the penetration depth of the magnetic field ($\lambda_\perp$), the vortex position (x), and the extension. The results obtained can be described in terms of the motion of a particle subjected to a potential $U(x, i_{dc}, \lambda_\perp)$, the analytical form of which is discussed as a function of the array parameters. Under certain circumstances, the injection of one vortex into the array may unleash a recursive process of vortex/antivortex creation that extends to the whole array. This gives rise to the formation of a stable dynamical state: the AVM (alternate-vortex motion), where vortices and antivortices move along alternate rows of plaquettes.

1. Introduction

2D arrays of Josephson junctions, JJA, have been the object of intense research for the last ten years. Besides their appeal as model systems for the study of the properties of 'granular' and 'stacked' superconductors, like the high-T_c superconductors, they are also interesting because of their intrinsically very rich physics. Moreover they are very promising systems for many technological applications in cryoelectronics.

The dynamical properties of Josephson junction arrays have been extensively studied in the past by several groups, theoretically and experimentally. Research in this field has evolved through an increasing complexity of the models studied toward a more realistic description of the JJA (including, e.g., the inductive effects [1]). Most of the efforts have been mainly focused on the dynamical steady state of the array as a function of the external field, the disorder of the array, etc [2].

Within this framework, the vortex dynamics has been studied numerically, analytically and experimentally. In most cases the theoretical study has been performed in the context of the sine–Gordon model, either in its continuous or discrete version, that respectively describe a long extended junction and a 1D array of parallel-shunted junctions [3]. Coupled sine–Gordon equations permit the modelling of the analogous 2D systems [4].

In this paper, instead, as an extension of previous work on the ladder dynamics, we focus our attention on the study of the single-vortex dynamics in 2D arrays of resistively shunted and overdamped Josephson junctions, described by the RSJ model. This problem

0953-8984/97/122571+13$19.50

is equivalent to the transmission of a perturbation through a system of coupled oscillators. Taking an interest in such a study is also partially motivated by the possible use of JJA in the development of cryoelectronics devices. Indeed superconducting networks allow a high-speed operation under very low power dissipation and are suitable for producing single-quantum-flux digital logic circuits [5], transistors [6], photofluxonic detectors [7], neural circuits [8], etc. Most of these applications are based upon the controlled creation and transmission of quantized excitations (vortices and/or antivortices), which act as information quanta. A quantitative study of the processes of creation and propagation of the signals is essential to the design of such cryodevices. To succeed in their reliable production one needs to know determining factors like the velocity of transmission of the vortex/antivortex, the scales of energy involved in the processes, and their dependence on the physical parameters—either external (e.g. the bias current supplied to the circuit, i_{ext}) or intrinsic to the array (i.e. the penetration depth of the magnetic field, $\lambda_\perp$).

In this paper we present a detailed study of dynamical quantities such as the vortex velocity, v, the coefficient of viscosity, η, and the height of the dynamical barrier for the cell-to-cell vortex motion, E_b. Their dependence on the vortex position (x), the bias current (i_{dc}) and the screening field (parametrized by $\lambda_\perp$) has been carefully worked out.

An array implies a discretization of the space—the length scale is given by a, the cell size—and thus an enhancement of the finite-size effects in the arrays whose dimensions, L_x and L_y, are not much greater than a. We have studied the dependence of the dynamical variables on the size of the array.

The dynamics of a single vortex in a 2D JJA can be described in terms of the motion of a particle subjected to an effective 1D potential $U(x, i_{dc}, \lambda_\perp)$, the shape of which will also be discussed in detail in this paper.

The paper is organized as follows. In section 2 we describe briefly the model used. In section 3 we describe the results that concern the vortex velocity, the damping coefficient and the energy barrier for the cell-to-cell vortex motion; they have all been worked out as functions of the relevant physical parameters of the array. In this section we also discuss the shape of the potential function U. In section 4, we describe processes that can prevent the use of JJA in applications strictly based upon the motion of single vortices: under particular physical conditions (e.g. above a given value of the bias current) the perturbation due to the presence and the motion of a vortex may induce vortex reflections at the border of the array and even, under certain circumstances, a truly vortex/antivortex cascade. In these conditions, at steady state, each row of the array exhibits a defined dynamical vorticity (i.e. a dominant presence of vortices or antivortices), the sign of which alternates from row to row: the so-called alternate-vortex motion (AVM) described in reference [9].

2. The model

For our studies we consider an ordered array with square plaquettes and one superconducting junction per link. The dynamics of the ladder is simulated in the limit of zero shunt capacity (i.e. the overdamped case). We also assume that the phase of the order parameter ϕ_i is constant on each grain (i.e. we consider point grains). The dynamical equations at $T = 0$ are [10]

$$\frac{\hbar}{2e}\sum_j \frac{1}{R_{ij}}\frac{\mathrm{d}}{\mathrm{d}t}(\phi_i - \phi_j - A_{ij}) = -\sum_j \sin(\phi_i - \phi_j - A_{ij}) + i_i(\mathrm{ext}) \qquad (1)$$

where i, j stand for nearest-neighbour points. $i_i(\mathrm{ext}) = I_i(\mathrm{ext})/I_c$ is the external current entering the site i normalized to the maximum critical current I_c, and R_{ij} is the shunt

resistance of the junction. In general, A_{ij} includes the contributions of both the external and the internal magnetic fields:

$$A_{ij} = \frac{2\pi}{\Phi_0} \int_i^j (\boldsymbol{a}_{ext} + \boldsymbol{a}_{int}) \, \mathrm{d}\boldsymbol{r} \tag{2}$$

where $\boldsymbol{a}$ is the vector potential, and Φ_0 the flux quantum. In this paper the external magnetic field is set to zero, and A_{ij} is entirely due to the currents circulating in the array (i_{ij}):

$$A_{ij} = \sum_k l \frac{1}{4\pi\lambda_\perp} FF_{ij;kl} i_{kl}. \tag{3}$$

Here FF is the inductance matrix [11] and $\lambda_\perp$ the penetration depth of the magnetic field normalized to the lattice spacing a, i.e. [12]

$$\lambda_\perp = \frac{1}{2\pi} \frac{\Phi_0}{\mu_0 I_c a} \tag{4}$$

A detailed description of the numerical algorithm is given in [13].

It is worthwhile noting that, since the knots of the array are represented by point grains, the fluxoid quantization is automatically fulfilled:

$$\sum_{ij\in\alpha} \theta_{ij} + \frac{2\pi}{\Phi_0}(f^{tot}) = 2n_\alpha\pi. \tag{5}$$

$\sum_{ij\in\alpha}$ stands for the anticlockwise sum along the links of the α-plaquette and θ_{ij} is the gauge-invariant phase along the link ij—restricted to the interval $(-\pi, \pi]$–. $f^{tot} = \sum_{ij\in\alpha} A_{ij}$ is the total flux through the cell.

The ladder is biased with an external d.c. current, parallel to the y-axis, $i_{ext} = i_{dc}$, that is injected at the top of the array ($y = (N_y - 1)/2$), and extracted at the bottom ($y = -(N_y - 1)/2$). Time is measured in units of the adimensional quantity t/τ, with $\tau = \hbar/(2eI_cR_{ij})$.

The creation of a single vortex is achieved through the temporary breaking of a link at the border of the ladder: the current surrounds the defect and induces an excess of vorticity in the rightmost plaquette leading to the vortex formation. After its creation, the vortex, subjected to the Lorentz force, moves along the array. This is a quite different experimental procedure from those adopted previously in reference [14], where the authors put the emphasis on the effects of various types of defect on the vortex dynamics.

3. Dynamical properties

Figure 1 shows different examples of vortex trajectories. We identify the position of the vortex with that of its centre, i.e. the cell with vorticity $n_\alpha = 1$ (see equation (5)). This is why in figure 1 the position of the vortex assumes discrete values.

We define the cell-average velocity $v(x)$ as $1/T_N$, where T_N is the time that the vortex spends in cell N; it is trivially related to the instantaneous velocity, $v_i(x)$, $v(x) = \langle v_i(t)\rangle_N$, where

$$\langle v_i(t)\rangle_N = a/(t_{N+1} - t_N) = \left(\int_{tN}^{tN+1} v_i(t) \, \mathrm{d}t\right) \Big/ (t_{N+1} - t_N).$$

A comparison between figures 1 and figures 2, where we have reported some examples of vortex profiles, clearly suggests a direct relation between the velocity and the spatial extension of the vortex.

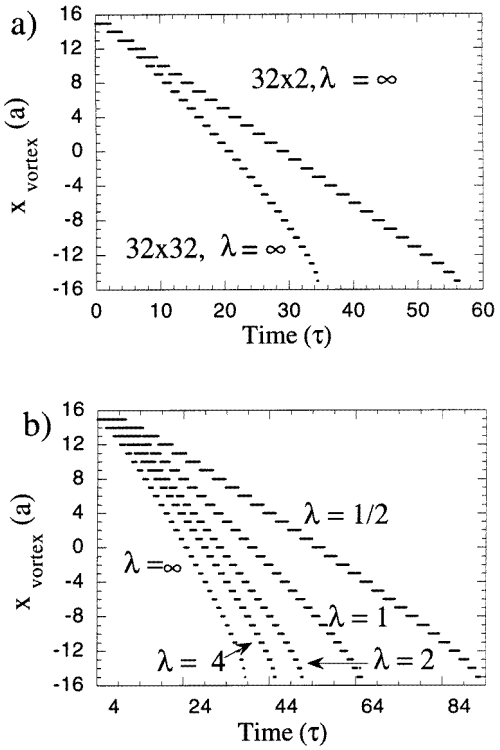

Figure 1. Examples of vortex trajectories: (a) as a function of the lattice size (we compare the motion of a vortex in a 32×2 cell ladder and in a 32×32 array); (b) as a function of the magnetic penetration depth $\lambda_\perp$ for a 32×2 cell ladder. Time is measured in units of $\tau = \hbar/(2eI_cR_{ij})$, and x in units of the lattice spacing a. $i_{dc} = 0.90$.

In a ladder (an array with $N_x \times 2$ sites), the transverse extension of the vortex is limited to a, the cell dimension, and this also affects its extension along the x-axis. In a large 2D array, however, this constraint does not exist and the degree of localization of the vortex depends on $\lambda_\perp$. In an $N_x \times N_y$ array, the radius of the vortex is a function of the length of the smallest side of the array (see figure 2(a)), and of the i_{dc}- and $\lambda_\perp$-values (figure 2(b)).

The shape of the $v(x)$ curve depends on the ratio of the vortex extension and the array size (see figure 3(a)): the vortex, created at the border of the array, initially accelerates until it is at a distance from the border greater than its extension. At this point it reaches a steady cell-average velocity v: v is no longer sensitive to the position and remains constant. When the vortex approaches the opposite border of the array, it accelerates again. In figure 3(a) we have fixed the smallest dimension of the array, $N_y = 32$. Thus the three curves correspond to vortices with the same extension. We note that the velocities at the centres of the array are basically the same in the three cases. If we reduce N_y (figure 3(b)) the $v(x)$ curve flattens, and the steady velocity decreases.

In figure 4 we report the steady velocity as a function of i_{dc} for different values of $\lambda_\perp$ in a 128×32 array. The smaller the vortex is, the lower its velocity is. An explanation of this behaviour will be provided below.

The motion of a vortex in a JJA can be nicely described in terms of that of a particle subjected to a given potential V. Let us analyse in detail the functional form of this potential

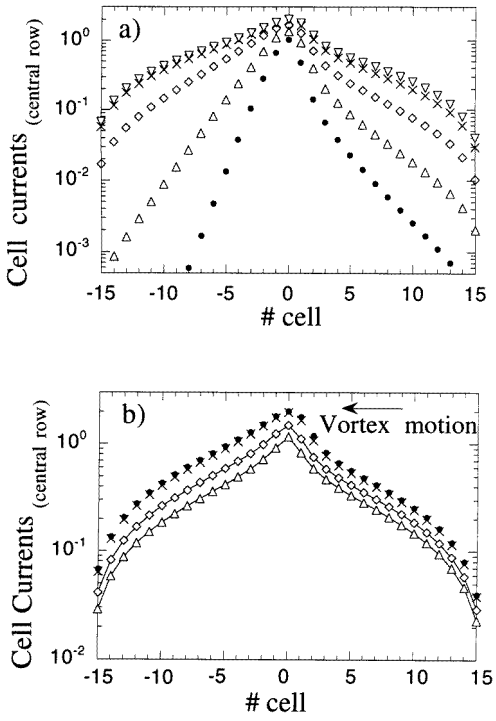

Figure 2. (a) The shape of a moving vortex as a function of the transverse size of the array for $32 \times N_y$ arrays ($N_y = 2$ (●), 4 (△), 8 (◇), 16 (×) and 32 (▽)). (b) The shape of a moving vortex as a function of $\lambda_\perp$ in a 32×32 array. $\lambda_\perp = \infty$ (●), 10 (×), 1 (◇) and 1/2 (△). The smallest dimension of the array determines the vortex extension. We plot the values of the mesh currents along the central row of the array (the vortex moves from right to left).

and its dependence on the array parameters.

The Gibbs energy of a certain phase configuration of a Josephson junction array is given by the following expression:

$$U = \sum_i i_{ext;i}\phi_i - \sum_{ij} \cos(\phi - \phi_j - A_{ij})$$

(if the screening effects are not negligible, then it is necessary to consider also the magnetic energy term: $\frac{1}{2} i_{ij} L_{ij;kl} i_{kl}$).

If we restrict ourselves to the study of the single-vortex dynamics, then we can identify V with U.

U can be decomposed into five terms [15]: the core energy $U_c = \pi^2/2$, defined as half the energy needed to create a vortex–antivortex pair; the energy of the vortex in the absence of a magnetic field and of external currents $U_0(x)$; the energies due to the interaction with the external field and with the bias current, $U_f(x)$ and $U_i(x)$; and the term that accounts for the periodicity of the ladder, $U_{pot}(x)$. Strictly speaking, U depends also on the vertical coordinate, y. In this paper, however, we will not study this dependence: we consider the case of a vortex that moves along the central row of the array ($y = 0$). Both the coordinates x and y are given in units normalized to the cell dimension, a.

The analytical expressions for $U_i(x)$, $U_f(x)$, and $U_{pot}(x)$ in terms of $\bar{h} I_c/(2e)$ are given

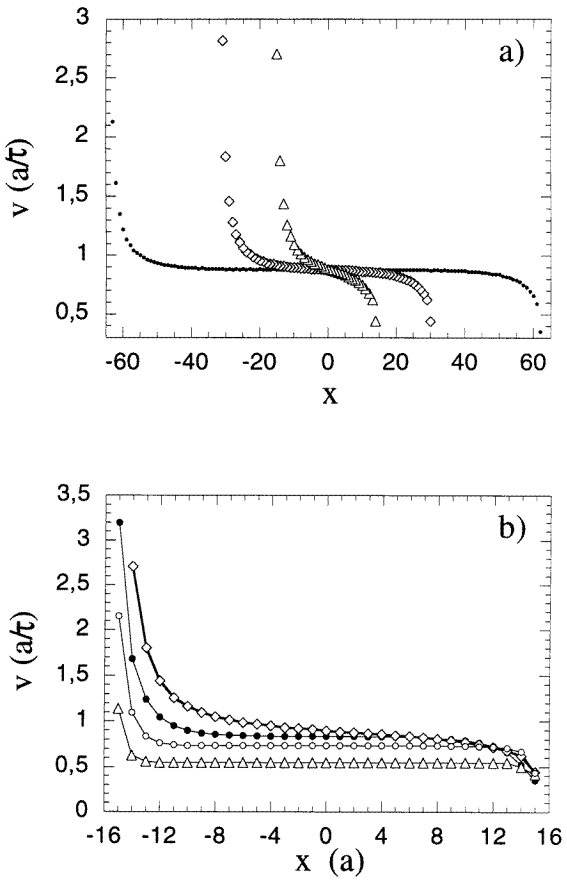

Figure 3. (a) $v(n)$ for $N_x \times 32$ arrays ($N_x = 32$ (△), 64 (◇), 128 (●)). $\lambda_\perp = \infty$, and $i_{dc} = 0.90$. The value of $v(0)$ is apparently the same in all cases. (b) $v(n)$ for square $32 \times N_y$ arrays (N_y = 2 (△), 4 (○), 8 (●) and 32 (◇)). The smallest dimension of the array determines the vortex extension and, thus, the profile and the steady value of the velocity.

respectively by

$$U_i(x) = -2\pi i(x + L/2) \tag{6}$$

$$U_f(x) = -\frac{\pi^2 L^2}{2} f\left(1 - 4\left(\frac{x}{L}\right)^2\right) \tag{7}$$

and

$$U_{pot}(x) = -\frac{1}{2} E_B \cos(2\pi x). \tag{8}$$

L is the array dimension of the direction perpendicular to that of the bias current normalized to the cell dimension, a, and E_B is the energy barrier that the vortex must overcome to move from one cell to the next one. We fixed the origin of the coordinates, $x = 0$, at the central column of the array.

We have checked that the i_{dc}-dependence of U is perfectly described by equation (6), independently of the size of the array and of the value of $\lambda_\perp$. Indeed, in figure 5(a) we

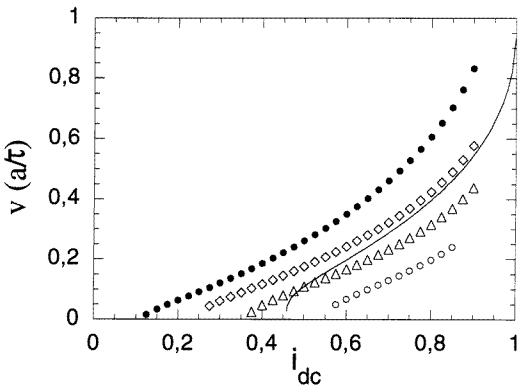

Figure 4. The steady vortex velocity, v, versus i_{dc} for different values of $\lambda_\perp$: ∞ (●), 2 (◊), 1 (△), 1/2 (○). Comparison is made with the results obtained for a ladder in the absence of inductance (continuous line).

show that $\int U(x)\,\mathrm{d}x$ fits very well to the expression $-2\pi i_{dc}L$, independently of the array parameters.

The functional form of $U_0(x)$ strongly depends on the vortex shape. For the case of a large 2D array, in the absence of inductive effects, it is given by

$$U_0(x) = \pi \ln\left(\frac{4L}{\pi^2}\cos\left(\frac{\pi x}{L}\right)\right). \tag{9}$$

Things change if the vortex extension is constrained by any means (a reduced size of the array, a small $\lambda_\perp$, etc). In order to check the spatial dependence of U_0 we have placed a vortex on different cells of the central row of the array. We have first initialized the phases to the expression $\arctan((y - y_0)/(x - x_0))$ and then let the system relax to the equilibrium configuration. In this way we place the vortex in the successive potential wells described by (8). Near the border, the slope of U_0 is so steep that a vortex is not a stable static configuration. We have compared these $U_0(x)$ values with the curve $U + 2\pi i_{dc}x$ (the continuous curve has been derived by fitting the discrete points) for 32×32 and 48×32 arrays. The results are shown in figure 5(b).

The effect of the array inductance is double. On one hand, it reduces the vortex energy (since the induced magnetic field tends to compensate the external one, the effective frustration decreases and so does the energy); on the other it modifies the energy profile, which gets flatter (this is because when $\lambda_\perp$ grows, the vortex extension decreases; U_0 becomes insensitive to the vortex position at a distance from the border greater than its radius).

A study of $U(x) + 2\pi i_{dc}x$ permits the determination of E_B from the spatial oscillations of the potential (see figure 5(b)). The results are shown in figure 6. A comparison is made with the E_B-values worked out for the case of a ladder; these latter turn out to be appreciably higher.

An intuitive argument explaining this behaviour is the following: if the vortex is strongly localized, the motion from one cell to the adjacent one implies a dramatic shift of all of the phases (especially of those along the links close to the plaquettes involved), and a higher energy is required in order to move the vortex.

It is worthwhile noting that the dynamical energy barrier is quite different from its statical value. In absence of inductance effects we have $E_B(\text{static}) = 0.2$ [16]. Phillips

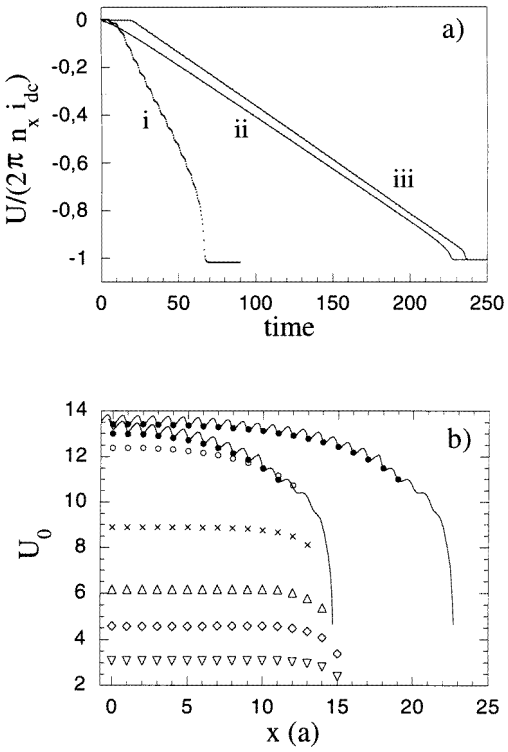

Figure 5. (a) $\int U/(N_x i_{dc})\,\mathrm{d}x$ during the vortex propagation: i: 16×16, $\lambda_\perp = 1$, $i_{dc} = 0.75$; ii: 128×32, $\lambda_\perp = \infty$, $i_{dc} = 0.75$; iii: 64×2 ladder, $\lambda_\perp = \infty$, $i_{dc} = 0.7$. It turns out that, independently of the size and the inductance of the array, the dominant component of U is $2\pi i_{dc} x$. (b) $U_0(x)$ in a 32×32 array, for different values of $\lambda_\perp$: 1/2 ($\triangledown$), 1 ($\Diamond$), 2 ($\triangle$), 32 ($\times$), and 64 ($\bigcirc$). We compare these values with those obtained for 32×32 and 48×32 arrays with $\lambda_\perp = \infty$ ($\bullet$). The continuous lines show $U + 2\pi i_{dc} x$ for a vortex moving in 32×32 and 48×32 arrays in the absence of inductance.

et al have generalized this result taking into account the screening effects: the energy barrier grows as $\lambda_\perp$ decreases, and for example $E_B(\text{static}, \lambda_\perp = 1) \approx 0.4$ [1]. These values are appreciably different from the values extrapolated from our curves for $v \to 0$. The difference between the dynamical and static values of the barrier energy can be qualitatively explained as follows: while the vortex is moving, the phase configuration does not have time to relax, and thus the dynamical E_B-results are greater than the static one. In addition, one has also to consider the extra contribution due to the energy supplied by the external current (we recall that the supplied power is $\sum_i i_i(\text{ext})\ \mathrm{d}\phi_i/\mathrm{d}t$); note that the Josephson energy, the externally supplied energy, and the magnetic energy all have their maxima when the vortex is located between two cells, so they all contribute with the same sign to the high value of E_B.

Let us now show how the vortex velocity can be derived from the potential U. In this paper we consider the zero-capacitance limit (the underdamped case), i.e. massless vortices. In consequence, the total force acting on the vortex is null, and

$$\frac{\partial U(x)}{\partial x} = -\eta v(x) \tag{10}$$

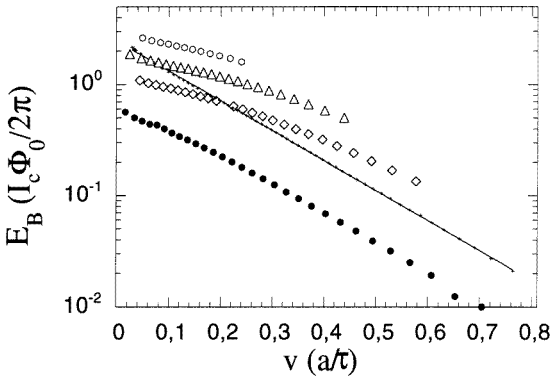

Figure 6. (a) E_B versus v. These values have been obtained by calculating both E_B and v for different values of i_{dc}. $\lambda_\perp = \infty$ (●), 2 (◊), 1 (△), 1/2 (○). Comparison is made with the results obtained in a ladder in the absence of inductance (continuous line).

where U and v are, respectively, the potential acting on the vortex and its velocity. Let us briefly recall how η can be calculated [17]: the power dissipated through all of the resistances of the array because of the vortex motion is given by $W_{diss} = \sum_{ij} V_{ij}^2/R_{ij}$ (we recall that, due to the energy conservation, $E_{diss} = -\sum_i i_{ext;i}\phi_i + \sum_{ij} \cos(\phi - \phi_j - A_{ij}) = -U$); of course $W_{diss} = \mathrm{d}E_{diss}/\mathrm{d}t$. We can define a damping coefficient η through $\eta v^2 = W_{diss}$. Let us focus our attention on the displacement of the vortex from a cell to the adjacent one, separated by a link ij. The phase of the link shifts by π in a time $\delta t = a/v$, where v is the vortex velocity. If R_{equiv} is the equivalent resistance of the circuit between the points i and j, the damping coefficient is given by

$$\eta = \Phi_0^2/(4a^2 R_{equiv}). \tag{11}$$

In the case of a large 2D array where all the resistances R_{ij} are equal, one has $R_{equiv} = R_{ij}/2$. In general, R_{equiv} is roughly defined by the dimension of the sub-array 'occupied' by the vortex, and it is thus dependent on the extension of this latter.

From (10) it is straightforward to obtain the instant vortex velocity $v_i(t)$, in the case of no array inductance:

$$v = \frac{1}{\eta_0}\left(2\pi i_{dc} + \frac{\pi^2}{N_x}\tan\left(\frac{\pi x}{N_x}\right) - \pi E_B \sin(2\pi x)\right). \tag{12}$$

Here η_0 is an adimensional quantity, related to η by $\eta = \eta_0\Phi_0^2/(4\pi^2 a^2 R_{ij})$.

Now we can qualitatively explain the dependence of the steady v on the array size. Near the centre—or, in rectangular arrays, far enough from the border—the spatial derivative of $U_0(x)$ can be neglected; as the integral of $\cos(2\pi x)$ along a plaquette is zero, the main contribution to the cell-average velocity comes from the i_{dc}-term, and does not depend on any other parameter. The larger the array is, the greater the equivalent resistance becomes: η decreases and thus the velocity increases. In an analogous way we can explain the decrease of v with an increasing $\lambda_\perp$: a low value of $\lambda_\perp$ implies a strong localization of the vortex, and thus a small R_{equiv}.

4. The vortex cascade

The control of the single-vortex propagation through the array is quite relevant for any practical applications. This is not always possible in the case of a 2D array: indeed the perturbation due to the presence and to the motion of the vortex may induce the creation of extra vortices/antivortices. This happens in arrays with more than one row of plaquettes. When the vortex (antivortex) is close enough to the border of the array it can induce the formation of antivortices (vortices), either in the row along which it is moving, or in the adjacent ones. This has been observed for bias currents greater than a threshold value, which is lower than the critical current of the array $i_{dc} = 1$.

The process is illustrated in figure 7: at $t = 0$ a vortex (black circle) is created in the central row of the array (row 0). The Lorentz force due to the bias current (we recall that the d.c. current is injected into the upper sites, and extracted from the lowest ones) makes the vortex move toward the left-hand border. At $t = 38\tau$, when the vortex is near the border, it induces the formation of three antivortices (open circles) in rows 0, 1 and -1, that begin to move to the right. The central antivortex annihilates with the original vortex; the other two, when approaching the opposite edge, induce the formation of new vortices, and so on. The energy of the system shows a peak whenever an annihilation occurs.

The extra vortex/antivortex creation process spreads from one row to the adjacent ones affecting, finally, the whole array. The result is that different rows exhibit a well-defined alternate vorticity (see figure 8, where we report the time-average number of vortices/antivortices in the array rows). This dynamical state, called alternate-vortex motion, has been recently observed by the Tübingen group [9] and confirmed by the numerical simulation of Hagenaars *et al* [18]. In their experiments, Lachenmann *et al* [9] scanned the sample with an electron beam; thus all of the links were perturbed. Our simulations show that, in order to unleash the process that leads to the AVM, it is enough to operate a perturbation on just one link of the array and wait for the appearance of the first free vortex. Once the free vortex has been created, provided that the bias current is higher than a certain critical value, the system, on its own, evolves towards the AVM.

5. Conclusions

In conclusion we have studied in detail the vortex transmission in 2D arrays of superconducting junctions. Dynamical variables such as the velocity, v, the damping coefficient, η, and the dynamical energy barrier, E_B, have been worked out as functions of the bias current, the magnetic penetration depth, the vortex position, and the extension.

The size of the system is a fundamental variable that deeply influences the vortex motion.

In a previous work [13] we have studied the vortex dynamics in a ladder, an array consisting of a single row of plaquettes. In that case, the small transverse length of the system constrained the vortex to be strongly localized. In 2D arrays, in contrast, the extension of the vortex is much larger.

(i) As a consequence the number of links affected by the vortex motion increases, and so does the equivalent resistance of the system, R_{equiv}, leading to a smaller damping coefficient, η. Since the dominant term of U depends just on i_{dc} (and it is independent from the lattice size), the vortex velocity increases with its size.

(ii) The more extended the vortex, the smoother the shift of the gauge-invariant phases as the vortex moves from cell to cell; this implies a decreasing of the energy barrier.

(iii) The spatial distribution of the different variables (velocity, energy, ...) is also

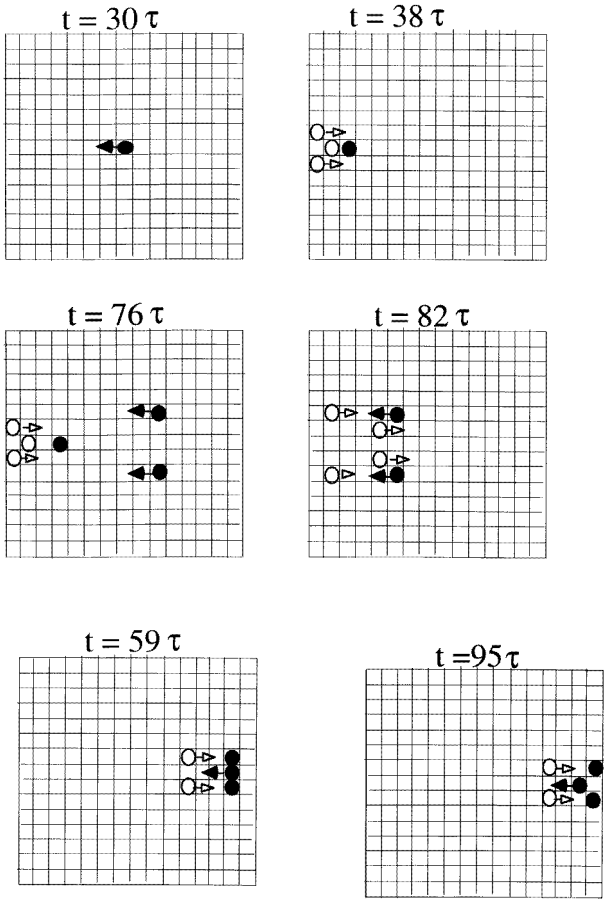

(a)

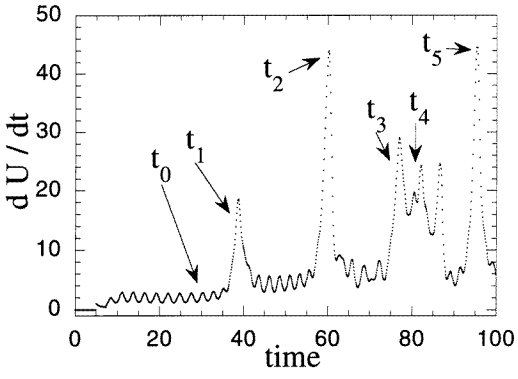

(b)

Figure 7. (a) The starting point of a vortex cascade. At $t = 0$ we inject a vortex in the central row of a 16×16 array, with $\lambda_\perp = 1$ and $i_{dc} = 0.9$, and leave the system to evolve on its own. The energy, the curve in (b), shows peaks whenever a vortex–antivortex annihilation occurs.

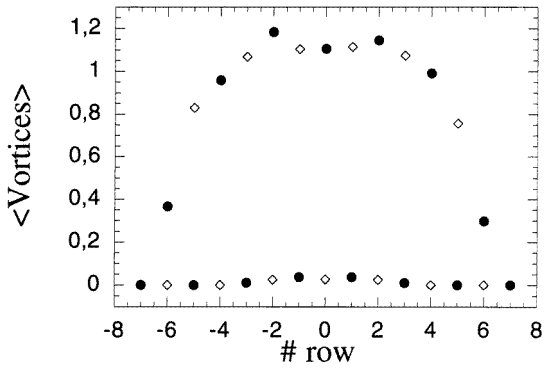

Figure 8. The time-average number of moving vortices (●) and antivortices (◊): rows with the dominant presence of vortices and antivortices alternate. We note that, for rows far from the central one, the average number of vortices/antivortices decays.

affected by the vortex extension: at distances from the border of the array greater than the extension, these variables are quite insensitive to the vortex position; however, near the borders, the slope of U gets steeper, causing the vortex to accelerate.

In addition:

(iv) we have shown that v and E_B depend not only on the size of the array, but also on the bias current and on the penetration depth of the array; indeed, v and E_B are respectively increasing and decreasing functions of i_{dc} and $\lambda_\perp$;

(v) we have illustrated the development of the vortex cascade process; the sufficient conditions for this are: an array with more than one row, and a high enough bias current. We stress that the vortex cascade can be unleashed by the injection of a single vortex.

Hence our conclusions are as follows.

(a) We remark that the study of the single-vortex dynamics, besides its interest as a theoretical problem, is relevant for practical implementations of arrays of Josephson junctions. In particular, most of the cryoelectronics devices are based upon the use of vortices or antivortices as travelling information quanta. Our dynamical results may be relevant for the design of such devices, as regards predicting their technical features (e.g. the velocity of transport of the signals), and stressing their drawbacks, such as the vortex/antivortex cascade. Processes like this latter may prevent the use of large 2D arrays in such applications.

(b) We stress that variables such as v or E_B are measurable quantities, so our results could be, in principle, experimentally checked by means of, e.g., low-temperature scanning electron microscopy (LTSEM) [9]. This technique allows one to measure time-averaged voltage fluctuations (ΔV) with a high spatial resolution. $\Delta V(x)$ can be related to the vortex/antivortex velocity at cell x. On the other hand, from the spatial variation of the velocity $v(x)$ it is possible to extract the value of E_B. The 'vortex cascade' process should also be easily observed.

Acknowledgment

J C Ciria acknowledges a post-doctoral grant provided by the MEC (Spain).

References

[1] Nakajima K and Sawada Y 1981 *J. Appl. Phys.* **52** 5732
Majhofer A, Wolf T and Dieterich W 1991 *Phys. Rev.* B **44** 9634
Domínguez D and José J V 1992 *Phys. Rev. Lett.* **69** 514
Phillips J R, van der Zant H S J, White J and Orlando T P 1993 *Phys. Rev.* B **47** 5219

[2] For a recent view on the state-of-the-art see, e.g.,
Giovannella C and Tinkham M (ed) 1995 *Macroscopic Quantum Phenomena and Coherence in Superconducting Networks* (Singapore: World Scientific)

[3] See, e.g.,
Pedersen N F and Ustinov A V 1995 *Supercond. Sci. Technol.* **8** 389
Nordman J E 1995 *Supercond. Sci. Technol.* **8** 681

[4] See, e.g.,
Ustinov A V 1995 *Macroscopic Quantum Phenomena and Coherence in Superconducting Networks* ed C Giovannella and M Tinkham (Singapore: World Scientific) p 253

[5] Likharev K K and Semenov V K 1991 *IEEE Trans. Appl. Supercond.* **1** 3
Nakajima K, Mizusawa H, Sugahara H and Sawada Y 1991 *IEEE Trans. Appl. Supercond.* **1** 29

[6] Berman D, van der Zant H S J, Orlando T P and Delin K A 1994 *IEEE Trans. Appl. Supercond.* **4** 1051

[7] Ciria J C, Pacetti P, Paoluzi L and Giovannella C 1996 *Nucl. Instrum. Methods* **370** 128
Giovannella C, Fontana A and Cikmach P 1991 *Magnetic Susceptibility of Superconductors and other Spin Systems* ed R A Hein, T L Francavilla and D H Liebenberg (New York: Plenum) p 455
Zhang Z M and Frenkel A 1994 *J. Supercond.* **7** 871

[8] See, e.g.,
Mizugaki Y, Nakajima K, Sawada Y and Yamashita T 1993 *Appl. Phys. Lett.* **62** 762 and references therein

[9] Lachenmann S G, Doderer T, Hoffmann D, Huebener R P, Booi P A A and Benz S P 1994 *Phys. Rev.* B **50** 3158

[10] Mon K K and Teitel S 1989 *Phys. Rev. Lett.* **62** 673
Chung J S, Lee K H and Stroud D 1989 *Phys. Rev.* B **40** 6570
Shenoy S R 1985 *J. Phys. C: Solid State Phys.* **18** 5163

[11] Nuvoli A, Giannelli A, Ciria J C and Giovannella C 1994 *Nuovo Cimento* **16** 2045

[12] Orlando T P, Mooij J E and van der Zant H S J 1991 *Phys. Rev.* B **43** 10 218

[13] Ciria J C and Giovannella C 1996 *J. Phys. C: Solid State Phys.* **40** 7463

[14] Cai Y, Leath P L and Yu Z 1994 *Phys. Rev.* B **49** 4015
Pacetti P, Ciria J C and Giovannella C 1994 *Nuovo Cimento* **16** 2039

[15] See, e.g.,
Van der Zant H S J, Rijken H A and Mooij J E 1983 *J. Low Temp. Phys.* **27** 150

[16] Lobb C J, Abraham D W and Tinkham M 1983 *Phys. Rev.* B **27** 150

[17] Rzchowski M S, Benz S P, Tinkham M and Lobb C J 1990 *Phys. Rev.* B **42** 2041

[18] Hagenaars T J, van Himbergen J E, Tiesinga P H E, José J V and Lachenmann S G 1995 *Macroscopic Quantum Phenomena and Coherence in Superconducting Networks* ed C Giovannella and M Tinkham (Singapore: World Scientific) p 329